Langmuir

Article

pubs.acs.org/Langmuir

Transition from Spherical to Irregular Dispersed Phase in Water/Oil Emulsions

M. Schmitt,[†] S. Limage,[†] D. O. Grigoriev,[‡] J. Krägel,[‡] V. Dutschk,[§] S. Vincent-Bonnieu,[∥,⊥] R. Miller,[‡] and M. Antoni*,[†]

[†]Aix-Marseille Université, CNRS, MADIREL UMR 7246, 13397 Marseille cedex 20, France

[‡]MPI of Colloids and Interfaces, Am Mühlenberg 1, 14476 Potsdam-Golm, Germany

[§]University of Twente, 7500AE Enschede, The Netherlands

[∥]European Space Agency, ESTEC, 2200AG Noordwijk, The Netherlands

ABSTRACT: Bulk properties of transparent and dilute water in paraffin oil emulsions stabilized with sodium dodecyl sulfate (SDS) are analyzed by optical scanning tomography. Each scanning shot of the considered emulsions has a precision of 1 μm. The influence of aluminum oxide nanoparticles in the structure of the water droplets is investigated. Depending on concentrations of SDS and nanoparticles, a transition occurs in their shape that changes from spherical to polymorphous. This transition is controlled by the SDS/alumina nanoparticles mixing ratio and is described using an identification procedure of the topology of the gray level contours extracted from each images. The transition occurs for a critical mixing ratio of $R_{crit} \approx 0.05$ which does not significantly depend on temperature and electrolyte concentration. This structural change seems to be a general feature when emulsifying dispersions and most probably involves both interfacial and bulk phenomena.

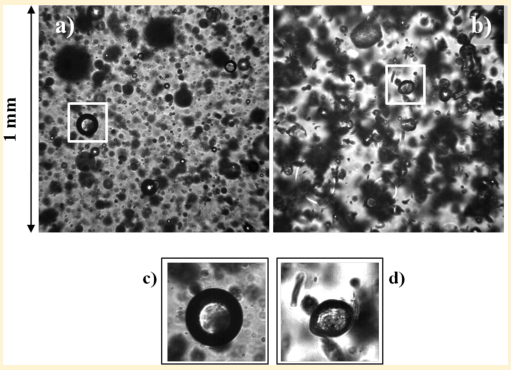

INTRODUCTION

Surfactants, polymers, proteins, and their mixtures can be used to create and stabilize foams and emulsions. For more than 100 years, it has been known that very small (micro- and nanometer sized) particles can act as stabilizers in emulsions. Ramsden described the formation of membrane-like thin film of solid particles which envelop both air bubbles and droplets in water, giving rise sometimes to "persistently deformed sharply angular and grotesque shapes of the emulsified globules".[1] Such particle-stabilized emulsions, which are now a topic of intensive research,[2−10] can be very stable due to the fact that the particles attach irreversibly to the water/oil interface. This yields a great mechanical stabilization of the droplets, even against Ostwald ripening.[11,12] A similar stabilization shows up in drop coalescence experiments.[13−16] The key factor for the use of particles as stabilizing agents in Pickering emulsions is their wetting by the two phases, oil and water.[17] But the characterization of nanoparticles in respect to their wetting properties is still an unsolved problem. It was shown[18] that a modified Wilhelmy plate method can be used for wettability characterization of alumina nanoparticles. Interesting buckling instabilities have also been observed during the compression or drying of particle-coated interfaces.[19−21]

Numerous fundamental questions arise to understand the structure of nanoparticle layers. For example, when charged latex particles of micrometer size are spread at an water/oil interface, they usually form a hexagonal lattice.[19] This is the sign that long-range repulsion prevents the particles from aggregating through van der Waals and capillary attractive forces. The physical nature of this interaction is still under discussion.[22] It is assumed that it is caused by the uneven distribution of electric charges of the particle across the water/oil interface. This asymmetry can induce an effective dipole normal to the fluid interface. The dipole−dipole repulsion through the oil phase is of much longer range than that through the water phase, where the interaction is screened due to the counterion condensation. Recently, it has been shown that a Coulombic repulsion through the oil phase could be responsible for the long-range repulsion of the particles.[19−22] For larger particles (>10 μm), the interface close to the particle can be deformed due to gravity, which causes then capillary interaction between the particles.[23,24] The balance between electrostatic repulsion and capillary attraction can cause the formation of remarkable structures at the water/oil interface. Horozov et al.[25,26] tuned the interactions between the particles at the interface by varying their hydrophobicity. As a result, the structure of the layers can be changed, as well as the rise of the surface pressure upon compression. Changing the size of the particles and using mixtures of particles could be another way to modify the structure of the layers.

Received: December 13, 2013
Revised: February 8, 2014
Published: March 4, 2014

   dx.doi.org/10.1021/la404766w | *Langmuir* 2014, 30, 4599−4604

One common way to tune the hydrophobicity of particles is the use of surfactants. The wetting conditions at the surface of solid particles indeed control their position in the liquid interfaces. The surface charge of particles can, for example, be tuned by the addition of opposite charged surfactants to modify their overall wetting properties. This can be easily achieved with negatively charged silica particles and a cationic surfactant like cetyltrimethylammonium bromide (CTAB). Ravera and co-workers[27,28] investigated the interfacial properties of such CTAB/silica particle mixtures in hexane-in-water emulsions. At a certain CTAB/silica particle mixing ratio, an irreversible attachment of the particles onto the fluid interface is observed. This phenomenon is followed by the formation of solidlike layers which modify the morphology of oil droplets in water based emulsions. Optical scanning tomography has been used to characterize properties of dilute water in paraffin oil emulsions.[29] When the volume fraction of such emulsions is small enough (typically smaller than 5%), they can appear as transparent media. The shape of the droplets they contain can then naturally be described by optical scanning tomography. In a previous work[30] we reported about such studies with colloidal silica dispersions with different amounts of CTAB to tune the hydrophobicity of silicon dioxide nanoparticles. The aim was to describe the influence of chemical composition in the structure of diluted water in paraffin oil emulsions. Optical tomography studies performed with different CTAB/silica particle mixing ratios suggest important qualitative changes at a critical CTAB/silica particle concentration ratio. A solidlike behavior appears for the interfaces similar to the ones of refs 27 and 28 that generates drastic changes of the droplet morphology when emulsified in paraffin oil emulsions. For the same emulsification protocol, the usual spherically shaped emulsion droplets become highly deformed and behave as stiff objects. To describe this effect, emulsions with different mixing ratios have been considered and analyzed with homemade image treatment routines. The introduction of a shape criterion allowed the description of the transition from spherical to polymorphic droplets. It has been shown that below a critical ratio droplets exhibit an irregular shape, while above this critical ratio droplets are spherical. Scanning electron microscopy (SEM)[31] and cryo-SEM investigations give some evidence that structure formation within the emulsified droplet can be one origin of the stabilization of the nonspherical droplets. A second source of nonspherical shape stabilization can be the bulk rheological behavior of the aqueous phase. As observed for cationic surfactant modified silica particles, the transitions from viscoelastic to viscous behavior complement the observations obtained by tomographic microscopy very well.[32] In ongoing experiments, such bulk rheological experiments are performed with the described systems.

The aim of this Article is to investigate the generality of these changes. It is indeed interesting to demonstrate that the actual structure of the emulsified droplets exhibits common characteristics independently of their chemical composition. To this end, we report about a study with an initially oppositely charged system where the aqueous solution consists in a mixture of aluminum oxide nanoparticles (Al_2O_3) modified with sodium dodecyl sulfate (SDS). This surfactant is used to tune the hydrophobicity of the positively charged Al_2O_3 nanoparticles. Dilute water + SDS + Al_2O_3 emulsions in paraffin oil are generated, and, as emulsions are transparent, optical scanning tomography is again used to characterize the shape of the droplets. The influence of alumina particles and SDS concentrations on the overall emulsion structure is investigated.

MATERIALS AND METHODS

Emulsions are formulated in two steps. Emphasis is first put on the preparation of the dispersed phase solutions (DPSs) that consists of a controlled mixture of alumina nanoparticles (Disperal powder supplied by the producer Sasol Germany), anionic surfactant SDS (Sigma Aldrich, 99%), water (HPLC grade), and eventually sodium chloride. According to the data provided by Sasol Germany,[33] Disperal is a synthetic boehmite alumina system produced from aluminum alkoxides. It is an acid dispersible powder with particle size of about 80 nm composed of smaller crystallites of 10 nm. Alumina content in Disperal is approximately 77%, indicating slightly higher water concentration than in the stoichiometric boehmite $[AlO(OH)]_2$. In an acidic medium, the dispersion exhibits excellent long-term stability due to the dissociation of two hydroxyl groups generating a large positive surface charge of the particles, with a zeta-potential close to +45 mV.

Alumina particles are first suspended in water and sonicated over 5 min in an ultrasonic bath. As mentioned above, the water used here may also contain a controlled NaCl concentration. After sonication, the value of the pH is adjusted to pH 3 using a 0.1 M HCl solution that is added dropwise upon continuous stirring. Before preparation of series of DPSs, two stock solutions of SDS, with concentrations 2 and 5.76 g/L, were prepared by dissolution of SDS in water that contains the same NaCl concentration as the one used previously for the alumina particles suspension. Corresponding pH values were also adjusted to approximately 3. DPSs are finally prepared by gradual dilution stock SDS solutions and aqueous alumina suspensions and finally mixed in 25 mL glass vials under continuous sonication in an ultrasound bath. Final pH of all of DPSs is controlled and remains set to pH 3.

In the following, the mixing ration R is defined as $R = [SDS]/[Al_2O_3]$. The DPSs were emulsified in paraffin oil (Fluka 76235) which has been used without further purification. The volume ratio DPS/paraffin oil in all investigated emulsions is fixed to 1%. Experiments were performed at room temperature (about 20 °C). Emulsification is achieved under a controlled protocol. The DPS is introduced in paraffin oil such that both phases were initially separated. This system is then degassed for 10 min under vacuum conditions. Emulsification is then achieved by magnetic stirring for 10 min at 800 rpm.

The resulting emulsions were finally transferred in 4 mL optical quartz cells for further analysis with optical tomographic microscopy.[29,30] This technique combines a classical microscope in transmitted light mode with a CMOS camera and an objective that are both on a translating stage. It is nonintrusive and allows a direct in situ description of the emulsions. As volume fraction is 1% and emulsification protocol is relatively gentle, the emulsions are always transparent in this study. It is then possible to investigate their properties inside the quartz cell, making therefore negligible all the perturbations due to solid/liquid interactions. In the following, images are captured almost in the middle of the emulsions at about 4−5 mm from the quartz cell walls. In its present configuration, the equipment used for this study allows tomographic shots of a volume of 1 mm^3 within 1 s with a spatial precision of 1 μm. Figure 1 shows two typical snapshots of two different emulsions that will be discussed in more details hereafter.

Finally, for the determination of the size distribution and size (zeta average) of Disperal particles as a function of SDS bulk concentration, dynamic light scattering measurements (DLS) were carried out by using a Zetasizer Nano-ZS instrument (model Zen 3500, Malvern, U.K.). Each value was obtained as average from three subsequent runs of the instrument with at least 15 measurements per run.

Image Treatment. For each scanning shot, a set of 500 images is generated. Qualitative features are extracted by a thresholding of the images and gray level contour identification. The acquired images represent 1 × 1 mm^2 pictures of the emulsion with a precision of 1024

dx.doi.org/10.1021/la404766w | Langmuir 2014, 30, 4599−4604

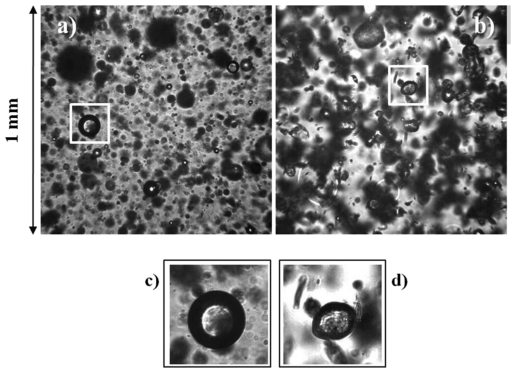

Figure 1. Examples of images obtained by optical tomographic microscopy: (a) 0.29 g/L SDS + 1.05 g/L Al_2O_3. $R \approx 0.28$ and droplets are spherically shaped. (b) 0.29 g/L SDS + 15.0 g/L Al_2O_3. $R \approx 0.02$ and droplets appear as polymorphous. (c, d) Magnification of the droplets in the white square frame of (a) and (b). [NaCl] = 0 g/L.

× 1024 pixels and gray level values between 0 and 255. Depth of field of the optics is about 30 μm. Each image can be considered as a surface where gray level value is the third coordinate. Depending on their shapes, droplets yield specific optical signals that will modify the overall shape of this surface. This basic idea is used to distinguish emulsions with spherical droplets from the polymorphous ones. The treatment of the images resulting from a given scanning shot is achieved in three steps: First, each image is smoothed using a 3 × 3 kernel to reduce the noise level. In the second step, 30 equidistant gray contour levels are used to treat each image. We note hereafter by $x_{GL}(i)$ the value of each of these gray levels for $i = 1$ to $i = 30$. This produces for each scanning shot a set of 10^6–10^7 contours that are stored for further treatment. This large number allows a statistical approach for their classification. This is the aim of the third step. Each contour is compared to a circle having exactly the same perimeter for the estimation of its standard deviation σ.[30] For spherical droplets, contours are close to circles and $\sigma \approx 0$, whereas for polymorphous ones contours are distorted and σ is large.

The way image treatment is addressed here makes possible the definition of a probability distribution function $F(x_{GL}(i),\sigma)$, that depends on both $x_{GL}(i)$ and σ and that determines the probability for a contour to have given standard deviation and gray level. Each emulsion is expected to have a signature that will generate a specific shape for F. The emulsion opacity and lighting conditions may influence this signature. A shift of the maximum of F in either dark or bright gray level domains might, for example, show up. This is why the gray levels are arbitrarily shifted in a way the average of F to be centered on gray level $x_{GL}(15) = 126$. The values of σ are on the other hand limited in the range $0 \leq \sigma \leq 5$ and sampled in 30 histogram bars. As 30 different values of the GLs are considered here, F will take values on a 30 × 30 grid and can be written $F(x_{GL}(i),x_\sigma(j))$, where

$$x_{GL}(i) = (i-1)E\left(\frac{256}{30}\right) \quad \text{and} \quad x_\sigma(j) = (j-1)\left(\frac{5}{30}\right)$$

where i and j are integers running from 1 to 30 and where function $E(x)$ stands for the integer part of x.

One difficulty here is to use an appropriate order parameter to identify the structure of the considered emulsion or, in other words, the level of distortion of the droplets. Such an order parameter is aimed to give a criterion of the deformation level of the droplets and therefore to allow to discriminate the emulsion structure. We propose in this work to define this order parameter from a reference emulsion with given SDS and NaCl concentrations but without alumina particles. All droplets are in this case spherical objects. Three different realizations of this reference emulsion are used to generate a reference probability distribution $F_{ref}(x_{GL}(i),x_\sigma(j))$. This function corresponds to emulsions with spherical droplets. Figure 2 displays its shape in the case [SDS] = 0.29 g/L and [NaCl] = 0 g/L. Once computed, F_{ref} is

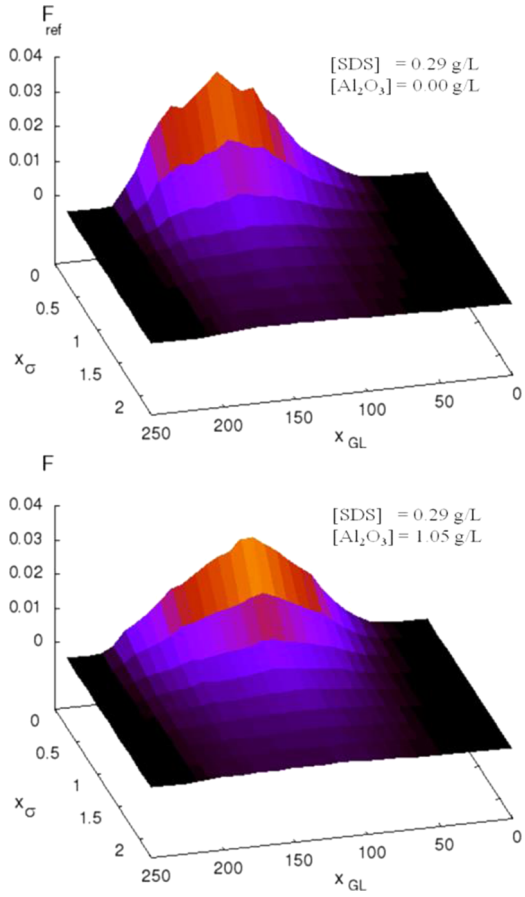

Figure 2. Reference probability distribution function F_{ref} for [SDS] = 0.29 g/L and [Al_2O_3] = 0 g/L, and shape of F for [SDS] = 0.29 g/L and [Al_2O_3] = 1.05 g/L. [NaCl] = 0 g/L.

used for the computation of the value of the order parameter, noted ξ, that reads:

$$\xi = \sum_{i=1}^{30}\sum_{j=1}^{30} |F_{ref}(x_{GL}(i), x_\sigma(j)) - F(x_{GL}(i), x_\sigma(j))|$$

F_{ref} and F are both normalized functions and therefore $0 \leq \xi \leq 1$. From this definition, small (respectively large) values of ξ will correspond to emulsions with spherical (respectively polymorphous) droplets. It is also important to note here that F_{ref} has to be recomputed when SDS and NaCl concentrations are changed. In the following, we limit our focus on DPSs with four (respectively three) different SDS (respectively NaCl) concentrations. For given SDS and NaCl concentrations, the alumina particles concentration is increased from 0 g/L (in the reference emulsions) up to a maximum of 5 g/L.

RESULTS AND DISCUSSION

Similarly to our previous study,[30] we will see in this section that the spherical-polymorphous droplet shape transition occurs at a relatively low mixing ratio: $R_{crit} \approx 0.05$. When $R > R_{crit}$, the emulsion contains predominantly spherical droplets, whereas for $R < R_{crit}$, this symmetry is lost and polymorphism rises. This is illustrated in Figure 3 that shows images of this transition for a constant SDS concentration of 0.03 g/L and increasing alumina particle concentrations. The transition from one emulsion type to the other is continuous. Spherical and polymorphous droplets indeed coexist in the emulsion when R remains close to R_{crit}. This work therefore provides only qualitative trends related to the predominant droplet geometry.

dx.doi.org/10.1021/la404766w | Langmuir 2014, 30, 4599–4604

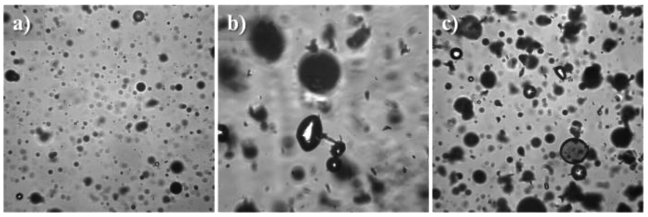

Figure 3. Images from tomographic microscopy for different alumina particle mixtures for a constant SDS concentration of 0.03 g/L. Spherical droplets in (a) for $[Al_2O_3]$ = 0.11 g/L ($R \approx 0.28$); the transition region in (b) for $[Al_2O_3]$ = 1.11 g/L ($R \approx 0.03$), and polymorphous droplets in (c) for $[Al_2O_3]$ = 15.0 g/L ($R \approx 0.002$). [NaCl] = 0 g/L.

It is important to stress here again that all emulsions where created with exactly the same protocol (see above). For $R \approx 0.28$ (Figure 3a), spherical droplets are formed, while for $R \approx 0.002$ (Figure 3c), both nonspherical and spherical droplets are created. In Figure 3b, for the ratio $R_{crit} \approx 0.03$, the transition from spherical to nonspherical shape is visible with a majority of large (50−200 μm radius) polymorphous droplets.

The value of R_{crit} is obtained from Figure 4 that shows a progressive change of ξ as a function of R. A clear modification

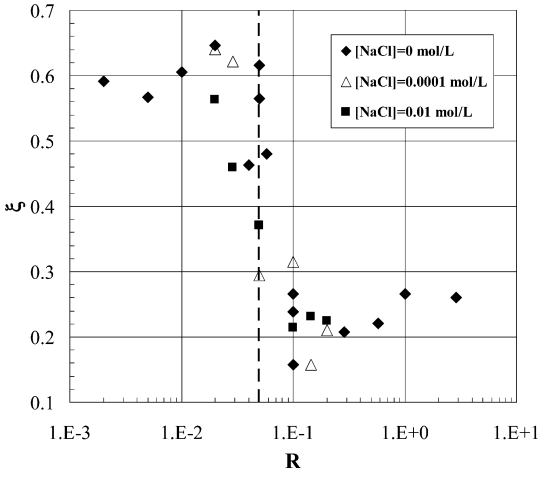

Figure 4. Parameter ξ as a function of R for different NaCl concentrations. The transition from spherical to polymorphous dispersed phase occurring for $R_{crit} \approx 0.05$ and is marked with dotted vertical line.

in the values of R can be identified when $R = R_{crit} \approx 0.05$. This is the sign that the emulsion structure is changed. Besides modifications of SDS and Al_2O_3 concentrations, two different NaCl concentrations (10^{-2} and 10^{-4} mol/L) are also considered. It appears that the addition of this salt has no significant influence on ξ and therefore on the value of R_{crit}.

Figure 5 gives an overview over emulsion structures as function of SDS and alumina nanoparticles concentrations. Both concentrations are expressed in grams per liter for simplicity. The dotted line corresponds to R_{crit}. Two composition domains are shown in this graph. Above the dashed line, all emulsions have their typical structure with spherical droplets. Below it, this symmetry is lost and emulsions display a more complex structure. This figure also indicates a larger dispersity as SDS concentration is increased. This can be seen by the lower contrast of the images when SDS concentration becomes higher. Figure 5 actually contains a

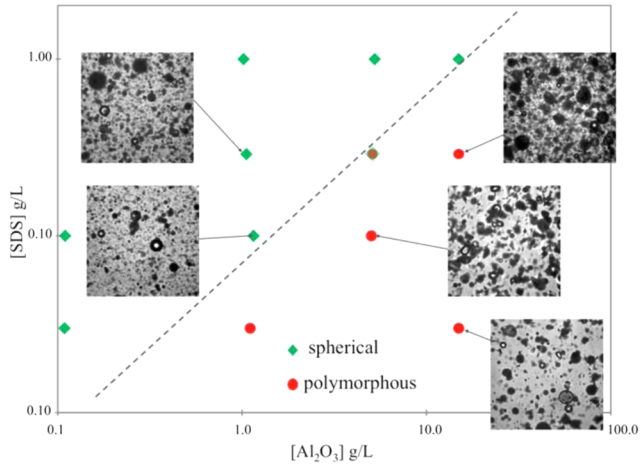

Figure 5. Transition from spherical to nonspherical shape. Dotted line is the critical mixing ratio between SDS and alumina particle. Microphotographs of five emulsions are displayed in insets corresponding to symbols on the graph. [NaCl] = 0 g/L.

third composition domain. Indeed, as alumina nanoparticles are not surface active, it is necessary to have a minimal amount of SDS to create emulsions. In this study, due to the emulsification protocol that is used, it was impossible to generate an emulsion when [SDS]<0.03g/L.

Figure 6a is a cryo-SEM image of a droplet obtained from an emulsion having the same composition as the one of Figure 3c. The water has been sublimated in order to visualize the droplet internal structure. Its volume actually appears to be completely filled with aluminum oxide nanoparticle layers that have been identified with X-ray spectroscopy. An enlargement of them is visible in Figure 6b. These layers are anchored into the water/paraffin oil interface where adsorbed microstructures can also be distinguished as illustrated by the arrows in Figure 6c. The previous observations have to be carefully handled as important artifacts are known to show up when freeze fracturing suspensions.[31] Still, it appears here that a large amount of nanoparticles remains inside the droplet and that a fraction of them is adsorbed on the water/paraffin oil interface.

The previous observations correlate with modifications of the surface charge of Disperal nanoparticles expressed in terms of their zeta potential as a function of R (Figure 7). As one can see, for ratios smaller than R_{crit} the droplets charge is rather insensitive to the SDS concentration in the mixture and their Zeta-potential remains at an almost constant level (about +45 mV). Approaching R_{crit}, however, causes a decay of charge with the isoelectric point between R = 0.1 and R = 0.2. Further increase of R leads to the Disperal charge inversion with values below −40 mV for $R > 1$. In this region, the almost completely neutralized particle surface charge allows formation of a second SDS adsorption layer around them due to hydrophobic interaction between the hydrocarbon tails.[34] This results in the increase of negative charge of particles and the recovery of the colloidal stability of the system.

The decrease of the absolute charge is associated to an increase of particle size in the suspension (Figure 8). Significant rise of size for $R \geq 0.05$ is a result of aggregation of initially fine particles with diameter of about 80 nm. In the range close to the isoelectric point the size of aggregates increases sharply up to some micrometers and the system becomes colloidally instable. It can be assumed that, in this region, alumina particles

dx.doi.org/10.1021/la404766w | Langmuir 2014, 30, 4599−4604

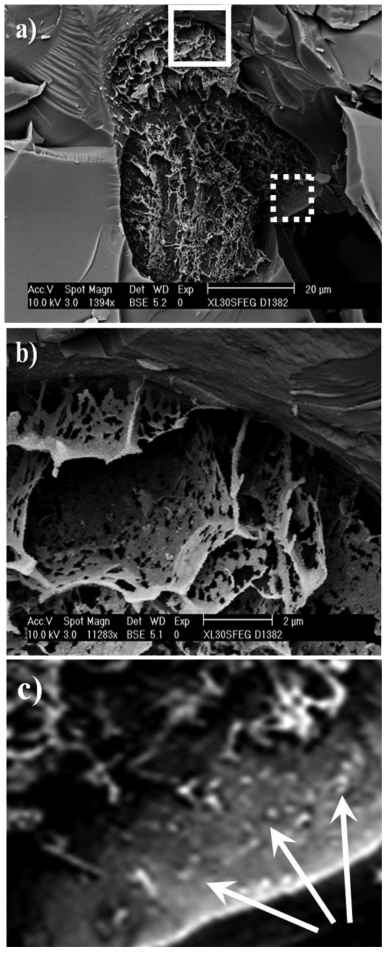

Figure 6. Cryo-SEM images of a droplet with [SDS] = 0.03 g/L and $[Al_2O_3]$ = 15 g/L ($R = 2 \times 10^{-3}$). Picture (a) shows a complete droplet. Picture (b) (respectively (c)) is a zoom inside the white full (respectively dashed) rectangle of (a).

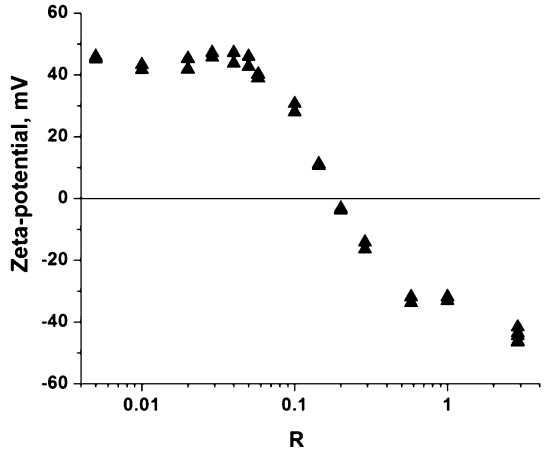

Figure 7. Zeta potential as a function of R ([NaCl] = 0 g/L).

can come much closer to each other since the electrostatic repulsion vanishes and can therefore form aggregates. The highest peak value shown in Figure 8 in the range $0.1 < R < 0.2$ reflects the appearance of aggregation mechanisms giving rise to larger aggregates. Interestingly, in this range of R values, spherical droplets are observed ($\xi \approx 0.2$). Further increase of SDS concentration for $R > 0.2$ leads on one hand to the

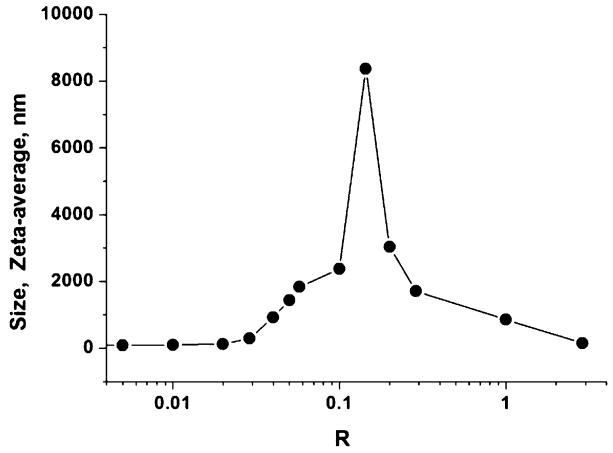

Figure 8. Size of alumina particles or aggregates obtained from DLS measurements as a function of R ([NaCl] = 0 g/L).

essentially lower size of dispersed particles which can be again measured quantitatively (Figure 8) and on the other hand to the weak increase of the droplets shape regularity (Figure 5). Nevertheless, the full re-establishment of the droplets' sphericity does not occur, indicating the irreversible character of the shape transition at R_{crit}.

When considering the dependency of ξ, zeta potential, and particle size on R (Figures 4, 7, and 8), one can propose at least a qualitative explanation for the droplet deformation phenomenon. Indeed, the progressive increase of particles hydrophobicity causes the rise of the particle attachment at the water/paraffin oil interface. Correspondingly, steadily decreasing particle charge enables closer and closer approach of particles and finally formation of particulate aggregates. Islands of aggregates can then adsorb at the interface and modify interfacial properties. Bulk properties of droplets probably also contribute. Cryo-SEM images indeed show the appearance of lamellar-like microstructures when $R < 0.05$. These microstructures consist of agglomerated nanoparticles and are known to be artifacts resulting from the freeze fracturing technique. They have therefore to be analyzed with caution. But one cannot exclude here colloidal-like microstructures to be also present at room temperature. If they bridge the droplets like in Figure 6, they might act as a stabilizing skeleton, explaining why polymorphism is high when nanoparticle concentration is large. Near the transition, cryo-SEM images indicate that microstructures become looser. When increasing R, they're progressively replaced by isolated aggregates that turn out to be too small and too few to fill the droplets. Bulk contributions become therefore weaker, allowing interfacial forces to overcome the stiffness of the droplets. This helps reduction of polymorphism and explains the ξ leveling off at a value of approximately 0.25. Charge reversal at $R > 0.2$ does not change the previous situation significantly. SDS concentration is then large enough for the molecules adsorbed on the nanoparticles to be organized in bilayers. At the water/paraffin oil interface, this will generate stronger charge repulsions through the oil phase without counterion screening. Destruction of droplet polymorphism is then promoted as well as detachment of the second SDS layer facing the paraffin oil phase. As a result, the particle surface at $R > 0.2$ can be imagined as SDS bilayers from the side of the aqueous phase with only surfactant monolayers directed toward the oil dispersion medium. This qualitative analysis can clearly be subject to further discussions. Overall,

dx.doi.org/10.1021/la404766w | *Langmuir* 2014, 30, 4599−4604

the still open question here is to understand whether the origin of droplet polymorphism results from droplet bulk, interfacial, or both bulk and interfacial phenomena.

CONCLUSIONS

This Article shows that particle-stabilized water-in-paraffin-oil emulsions can exhibit different structures and sharp changes in the shape of the dispersed phase. In our previous study, a similar behavior has been observed for negatively charged particles modified by a cationic surfactant.[30] This trend has been confirmed here by a study with positively charged alumina nanoparticles modified by SDS. The control parameter is the SDS/alumina nanoparticles mixing ratio R. The change in the emulsion structure shows up when this ratio takes the value $R = R_{crit} \approx 0.05$. Depending on whether the considered mixing ratio is above or below this value, the emulsions show either the usual equilibrium structure with spherically shaped droplets or strongly deformed ones. In this last case, droplets behave as stiff objects. The investigation of the alumina nanoparticles surface charge and aggregation as a function of R indicates strong modifications when the mixing ratio is close to R_{crit}. This change is qualitatively explained by invoking a possible interplay between droplet bulk and interfacial phenomena.

AUTHOR INFORMATION

Present Address

[⊥]S.V.-B.: Currently at Shell GSI, Rijswijk, The Netherlands.

Notes

The authors declare no competing financial interest.

ACKNOWLEDGMENTS

This work was partially supported by CNES, COST actions MP1106 and CM1101, the DFG SPP 1506 Mi 418/18-2, ESA MAP-FASES/PASTA, GdR-CNRS MFA, and Mousses et Emulsions.

REFERENCES

(1) Ramsden, W. *Proc. R. Soc. London* **1903**, *72*, 156−164.
(2) Horozov, T. S. *Curr. Opin. Colloid Interface Sci.* **2008**, *13*, 134−140.
(3) Hunter, T. N.; Pugh, R. J.; Franks, G. V.; Jameson, G. J. *Adv. Colloid Interface Sci.* **2008**, *137*, 57−81.
(4) Park, B. J.; Furst, E. M. *Langmuir* **2008**, *24*, 13383−13392.
(5) Synytska, A.; Ionov, L.; Dutschk, V.; Stamm, M.; Grundke, K. *Langmuir* **2008**, *24*, 11895−11901.
(6) Whitby, C. P.; Fornasiero, D.; Ralston, J. *J. Colloid Interface Sci.* **2008**, *323*, 410−419.
(7) Zhang, S.; Lan, Q.; Liu, Q.; Xu, J.; Sun, D. *Colloids Surf., A* **2008**, *317*, 406−413.
(8) Vignati, E.; Piazza, R.; Lockhart, T. P. *Langmuir* **2003**, *19*, 6650−6656.
(9) Giermanska-Kahn, J.; Schmitt, V.; Binks, B. P.; Leal-Calderon, F. *Langmuir* **2002**, *18*, 2515−2518.
(10) Binks, B. P.; Lumsdon, S. O. *Langmuir* **2000**, *16*, 8622−8631.
(11) Aveyard, R.; Clint, J. H.; Horozov, T. S. *Phys. Chem. Chem. Phys.* **2003**, *5*, 2398−2409.
(12) Melle, S.; Lask, M.; Fuller, G. G. *Langmuir* **2005**, *21*, 2158−2162.
(13) Stancik, E. J.; Kouhkan, M.; Fuller, G. G. *Langmuir* **2004**, *20*, 90−94.
(14) Stancik, E. J.; Fuller, G. G. *Langmuir* **2004**, *20*, 4805−4808.
(15) Horozov, T. S.; Aveyard, R.; Clint, J. H.; Neumann, B. *Langmuir* **2005**, *21*, 2330−2341.
(16) Ashby, N. P.; Binks, B. P.; Paunov, V. N. *Chem. Commun.* **2004**, 436−437.
(17) Pickering, S. U. *J. Chem. Soc., Trans.* **1907**, *91*, 2001−2021.
(18) Dutschk, V.; Stöckelhuber, W.; Albrecht, V.; Geissler, U.; Simon, F.; Petzold, G.; Bellmann, C. *Nuremberg Proceedings*, 2007.
(19) Aveyard, R.; Clint, J. H.; Nees, D.; Paunov, V. N. *Langmuir* **2000**, *16*, 1969−1979.
(20) Xu, H.; Melle, S.; Golemanov, K.; Fuller, G. *Langmuir* **2005**, *21*, 10016−10020.
(21) Tsapis, N.; Dufresne, E.; Sinha, S.; Riera, C.; Hutchinson, J.; Mahadevan, L.; Weitz, D. *Phys. Rev. Lett.* **2005**, *94*, 018302.
(22) Aveyard, R.; Binks, B. P.; Clint, J. H.; Fletcher, P. D. I.; Horozov, T. S.; Neumann, B.; Paunov, V. N.; Annesley, J.; Botchway, S. W.; Nees, D. *Phys. Rev. Lett.* **2002**, *88*, 246102.
(23) Kralchevsky, P. A.; Nagayama, K. *Adv. Colloid Interface Sci.* **2000**, *85*, 145−192.
(24) Kralchevsky, P. A.; Denkov, N. D. *Curr. Opin. Colloid Interface Sci.* **2001**, *6*, 383−401.
(25) Horozov, T. S.; Aveyard, R.; Clint, J. H.; Binks, B. P. *Langmuir* **2003**, *19*, 2822−2829.
(26) Horozov, T. S.; Binks, B. P.; Aveyard, R.; Clint, J. H. *Colloids Surf., A* **2006**, *282*−*283*, 377−386.
(27) Ravera, F.; Santini, E.; Loglio, G.; Ferrari, M.; Liggieri, L. *J. Phys. Chem. B* **2006**, *110*, 19543−19551.
(28) Ravera, F.; Ferrari, M.; Liggieri, L.; Loglio, G.; Santini, E.; Zanobini, A. *Colloids Surf., A* **2008**, *323*, 99−108.
(29) Antoni, M.; Krägel, J.; Liggieri, L.; Miller, R.; Sanfeld, A.; Sylvain, J. D. *Colloids Surf., A* **2007**, *309*, 280−285.
(30) Schmitt-Rozières, M.; Krägel, J.; Grigoriev, D. O.; Liggieri, L.; Miller, R.; Vincent-Bonnieu, S.; Antoni, M. *Langmuir* **2009**, *25*, 4266−4270.
(31) Limage, S.; Schmitt, M.; Vincent-Bonnieu, S.; Dominici, C.; Antoni, M. *Colloids Surf., A* **2010**, *365*, 154−161.
(32) Limage, S.; Krägel, J.; Schmitt, M.; Dominici, C.; Miller, R.; Antoni, M. *Langmuir* **2010**, *26*, 16754−16761.
(33) Sasol Germany. http://www.sasolgermany.de/fileadmin/doc/alumina/DISPERAL-DISPAL.GB_04.pdf.
(34) Wang, W.; Gu, B.; Liang, L.; Hamilton, W. A. *J. Phys. Chem. B* **2004**, *108*, 17477−17483.